Cellular/Molecular

# Control of Rhodopsin's Active Lifetime by Arrestin-1 Expression in Mammalian Rods

**Owen P. Gross and Marie E. Burns**
Department of Ophthalmology & Vision Science, Center for Neuroscience, University of California, Davis, Davis, California 95618

**In rod photoreceptors, deactivation of the light-activated G-protein-coupled receptor rhodopsin (R*) is initiated by phosphorylation and completed through subsequent binding of visual arrestin (Arr1). The *in vivo* kinetics of these individual interactions have proven difficult to determine with precision since R* lifetime is much shorter than the lifetimes of downstream G-protein and effector molecules. Here, we have used a transgenic mouse line with accelerated downstream deactivation kinetics to reveal the contribution of Arr1 binding to the overall time course of rhodopsin deactivation. Photoresponses revealed that the lifetime of R* is significantly increased in rods that express half of the normal amount of Arr1, in a manner consistent with a twofold decrease in the rate of Arr1 binding across a wide range of flash strengths. A basic model of photoresponse deactivation consistent with established photoreceptor biochemistry shows that R* phosphorylation and Arr1 binding occur with a time constant of ~40 ms in wild-type mouse rods, much faster than previous estimates.**

## Introduction

In nearly all eukaryotic cells, deactivation of G-protein-coupled receptors determines the balance between signal amplification and timely response recovery. In the G-protein cascade of retinal rods, photoexcited rhodopsin (R*) activates the G-protein transducin ($G_t\alpha$) at a rate of several hundred per second (Heck and Hofmann, 2001; Arshavsky et al., 2002) throughout its active lifetime, providing the amplification needed for single-photon detection. Prolonging R* lifetime by interfering with deactivation mechanisms, which include phosphorylation by GRK1 and final quench by the binding of visual arrestin (Arr1), slows recovery of the outer segment light response (Xu et al., 1997; Chen et al., 1999; Mendez et al., 2000; Doan et al., 2006; Chan et al., 2007). However, the normal active lifetime of R* as determined by these deactivation mechanisms remains one of the fundamental unsolved puzzles in phototransduction.

Defining the individual contributions of phosphorylation and Arr1 binding to R* deactivation in normal rods has been challenging because phosphorylation both reduces R* activity and increases the affinity for Arr1 binding (Palczewski et al., 1992; Krupnick et al., 1997; Xu et al., 1997; Gurevich, 1998; Gibson et al., 2000; Vishnivetskiy et al., 2007). Overexpression of GRK1 has no effect on the amplitude or time course of the light response (Krispel et al., 2006; Whitcomb et al., 2009), indicating that GRK1 expression does not rate-limit R* deactivation. Underexpression of Arr1 similarly has no consequences for the duration of the single-photon response (Xu et al., 1997), suggesting that Arr1 binding also does not rate-limit R* deactivation. The apparent lack of effect of both GRK1 and Arr1 expression on the time course of the dim flash response might arise because R* deactivation is much faster than the deactivation of downstream G-protein/effector molecules ($G_t\alpha$/PDE) (Krispel et al., 2006; Burns and Pugh, 2009; Chen et al., 2010). Thus, we reasoned that the kinetics of the dim flash response would be more sensitive to small changes in R* lifetime in rods with accelerated $G_t\alpha$ GTPase activity, such as those that overexpress the RGS9 complex (Krispel et al., 2006).

To test this idea, we have recorded from rods with normal and reduced Arr1 expression in the RGS9-overexpression (RGS9-ox) background. Our results in both wild-type and RGS9-ox backgrounds support the conclusion that decreased Arr1 expression indeed leads to a slowing of R* deactivation and provide new estimates of the rate of phosphorylation and Arr1 binding in intact mouse rods.

## Materials and Methods

*Use of experimental animals.* Mice were cared for and handled following an approved protocol from the Institutional Animal Care and Use Committee of the University of California, Davis, and in compliance with National Institutes of Health guidelines for the care and use of experimental animals. Control mice in this study consisted of adult wild-type C57B/6 mice (Charles River) and R9AP138 transgenic mice (fourfold overexpressors; Krispel et al., 2006). Mice hemizygous for Arr1 were obtained by breeding each of these control strains with *Arr1*−/− mice (Xu et al., 1997). Genotypes were determined by PCR analysis as previously described (Xu et al., 1997; Krispel et al., 2006).

*Isolation of rod outer segments.* Approximately 12 retinas were harvested in darkness from dark-adapted mice of each genotype (WT or *Arr1*+/−) and vortexed in 2% OptiPrep (Sigma). This preparation was centrifuged through a gradient of 8%, 12%, 16%, and 20% OptiPrep for 20 min, which resulted in three visibly distinct bands of tissue in the gradient. The bottom two bands were collected, filtered, pelleted, and washed in Ringer's solution (130 mM NaCl, 3.6 mM KCl, 2.4 mM $MgCl_2$, 1.2 mM $CaCl_2$, 10 mM HEPES, and 0.2 mM EDTA). The final product was stored in the dark at −80°C.

Received Oct. 30, 2009; revised Jan. 15, 2010; accepted Jan. 20, 2010.

This work was supported by National Eye Institute Grants EY014047 (R01 to M.E.B.) and EY015387 (Training Program in Vision Science in partial support of O.P.G.). We thank E. N. Pugh Jr for critically reading this manuscript.

Correspondence should be addressed to Marie E. Burns, Center for Neuroscience, University of California, Davis, 1544 Newton Court, Davis, CA 95618. E-mail: meburns@ucdavis.edu.

DOI:10.1523/JNEUROSCI.5391-09.2010

 0270-6474/10/303450-08$15.00/0

*Quantitative Western blotting.* A freshly isolated, dark-adapted mouse retina or a frozen pellet of isolated mouse ROS was homogenized in Ringer's solution and maintained at 4°C in the dark. An aliquot of the homogenate was then added to a solution containing 70 mM *n*-octylglucoside and 50 mM hydroxylamine, pH 7.4. The rhodopsin content of the solution was determined by measuring the absorptivity at 500 nm before and after a full bleach assuming the extinction coefficient $\varepsilon = 40{,}500$. The remaining homogenate was then diluted in sample buffer so that the final concentration of rhodopsin was 1.0 $\mu$M. To facilitate comparisons, tissue samples from WT and transgenic retinas were processed together for Western blots: samples were subjected to twofold serial dilutions, separated by SDS-PAGE, and transferred to PVDF membrane (Bio-Rad). Blots were incubated with either rabbit anti-Arr1 (178605, Calbiochem), mouse anti-RK (MA1-720, Affinity Bioreagents), or rabbit anti-$G_t\alpha$ (sc-389, Santa Cruz Biotechnology) and the appropriate secondary antibodies conjugated to IR dyes (Invitrogen). Signals were detected and quantified with a Li-Cor Odyssey system.

*Electrophysiology.* All mice were reared in 12 h cyclic light. On the day of an experiment, an adult mouse that had been dark adapted overnight was killed with $CO_2$ and decapitated under infrared light. One retina was dissected and processed for Western blotting, and the other retina was stored in Leibovitz's medium (L-15; Invitrogen) on ice for suction electrode recordings in bicarbonate-buffered Locke's solution at 36 ± 1°C as previously described (Keresztes et al., 2004). Because a recent report promoted the idea that R* lifetime is longer than $G_t\alpha$/PDE in rod responses recorded in Ames' medium at 30°C, some experiments were executed with the precise storage and recording conditions described by the protocol in the Materials and Methods of that report (Doan et al., 2009). The results of these experiments are reported in the supplemental material (available at www.jneurosci.org).

The average number of photoisomerizations per flash ($n$) was calculated with variance-to-mean analysis from an ensemble of at least 25 responses to dim flashes, which by definition had amplitudes that were <20% of the maximal response amplitude (Rieke and Baylor, 1998). The average single-photon response was determined by dividing the average dim flash response by $n$.

We empirically calculated the effective collecting area for each rod by dividing $n$ by the flash strength [in photons per square micrometer (Baylor et al., 1979)]. The average effective collecting area of wild-type rods (0.34 ± 0.03 $\mu m^2$, $n = 18$) was slightly larger ($p < 0.03$) than those of *Arr1+/−* (0.24 ± 0.03 $\mu m^2$, $n = 18$), RGS9-ox (0.22 ± 0.02 $\mu m^2$, $n = 16$), and *Arr1+/−* $^{RGS9\text{-}ox}$ rods (0.24 ± 0.03 $\mu m^2$, $n = 33$). For each rod, the effective collecting area was multiplied by a known flash strength to calculate the number of R*/flash for Figure 4.

*Calculation of single-photon response time-dependent variance.* To identify individual single-photon responses (SPRs), the average dim flash response was converted to a template (Baylor et al., 1979) by normalizing the peak amplitude to 1.0 and truncating the response after the first 250 ms following the flash. Each individual dim flash response was assigned a scaling factor determined by the value of the cross-correlation of the response with the template at the time point of the flash. A histogram was constructed from these scaling factors, yielding a Poisson distribution, and SPRs were differentiated from failures and multiple photoisomerizations by the local minima on either side of the first peak not centered at zero (Rieke and Baylor, 1998). The response average and time-dependent variance were calculated for the isolated SPRs of each rod. Four *Arr1+/−* and four wild-type rods were selected so that the subpopulation mean SPRs had similar peak amplitudes. The average time-dependent variances for these subpopulations are shown in Figure 2*C*.

*Determination of time required for dominance: defining "sufficiently late times" for measuring deactivation kinetics.* The recovery of the rod OS photoresponse in dim and saturating flash regimes follows the decline of $G_t\alpha$/PDE, which was first approximated as the convolution of two exponentials:

$$E^*(t) = (e^{-t/\tau_R}) * (\nu_{RE} e^{-t/\tau_E}). \quad (1)$$

Here, $\tau_R$ and $\tau_E$ are time constants for the decay of R* and $G_t\alpha$/PDE, while $\nu_{RE}$ is the rate constant for $G_t\alpha$/PDE activation by R* (Pugh and Lamb, 1993). Under this framework, $E^*(t)$ approximates a single-exponential decay function with a time constant $\tau_D = \tau_E$ at sufficiently late times (Nikonov et al., 1998). We developed a mathematical method to define "sufficiently late times" given values of $\tau_R$, $\tau_E$, and a term for the experimental uncertainty (Eq. 4; supplemental material, available at www.jneurosci.org). Once dominance is established, Equation 1 reduces to the following:

$$E^*(t) \approx \nu_{RE}\left(\frac{1}{\tau_R} - \frac{1}{\tau_E}\right) e^{-t/\tau_E}. \quad (2)$$

The vertical shift in saturation times ($\Delta t$) resulting from an increase in $\tau_R$ associated with underexpression of *Arr1+/−* (Fig. 4) can be used to calculate the time constant for the decay of R* in *Arr1+/−* rods by setting $E^*(t;\tau_R^{wt}) = E^*(t + \Delta t;\tau_R^{+/-})$:

$$\tau_R^{+/-} = \left[\frac{1}{\tau_E} + \left(\frac{1}{\tau_R^{wt}} - \frac{1}{\tau_E}\right) e^{-\Delta t/\tau_E}\right]^{-1}. \quad (3)$$

The small difference between $\tau_R^{wt}$ and $\tau_R^{+/-}$ permitted by Equation 3 partially motivated our adoption of the two-time constant model for R* deactivation (Eq. 5).

## Results

### Arr1 concentration is reduced in *Arr1+/−* rod outer segments

Previous quantifications of Arr1 content in *Arr1+/−* retinas have resulted in values varying from 33% to 47% of that found in WT retinas (Xu et al., 1997; Hanson et al., 2007a; Doan et al., 2009), and immunohistochemical quantification of Arr1 compartmentalization suggested that a similar proportion of the overall Arr1 content is localized to the OS in rods with normal and reduced Arr1 expression (Hanson et al., 2007a). To understand the effects of reduced Arr1 expression on rod flash responses, it was first necessary to quantify the levels of Arr1 protein in the dark-adapted OS of the *Arr1+/−* mice in our colony. Thus, we performed quantitative Western blots on both whole retinal homogenates and purified rod outer segments (ROS) from dark-adapted *Arr1+/−* mice. We found that Arr1 expression in retinas of *Arr1+/−* mice was half that of WT retinas (ratio to WT expression = 0.51 ± 0.01 for *Arr1+/−*; $n = 4$) (Fig. 1*A*,*D*). A similar test performed on purified ROS from *Arr1+/−* mice demonstrated that a reduction in overall Arr1 expression results in a reduction in OS Arr1 content of similar scale (supplemental Fig. S1, available at www.jneurosci.org as supplemental material), although this purification method is unlikely to provide a precise quantification of Arr1 since it is vulnerable to inner segment contamination and therefore less reliable than previous results (Hanson et al., 2007a). We conclude that the amount of Arr1 in the OS is a fixed percentage of the cell's total Arr1 protein, and thus there does not seem to be a mechanism to maintain a fixed ratio of Arr1:rhodopsin in dark-adapted OS.

To test whether changes in the expression of GRK1 and $G_t\alpha$ might compensate for the reduction of Arr1 in *Arr1+/−* rods, we performed quantitative Western blots of wild-type and *Arr1+/−* retinas, but found no significant differences (data not shown), consistent with previous reports (Doan et al., 2009). Furthermore, Arr1 levels in RGS9-overexpressing rods were normal (ratio to WT expression = 1.10 ± 0.05; $p = 0.25$ compared to WT; $n = 5$) (Fig. 1*B*,*D*), and Arr1 was similarly reduced in *Arr1+/−* $^{RGS9\text{-}ox}$ retinas as in *Arr1+/−* retinas (ratio to WT expression = 0.56 ± 0.05; $n = 5$; $p = 0.37$ compared to *Arr1+/−*) (Fig. 1*C*,*D*). The results of these Western blot experiments led us to conclude that the effects of Arr1 underexpression could be best

addressed by returning to electrophysiology, first to develop a more complete characterization of the responses of *Arr1*+/− rods, and then to test whether the normally slower $G_t\alpha$/PDE deactivation masks the consequences of a reduced rate of Arr1-R* binding in rods with reduced Arr1 expression.

### Reduced Arr1 expression slows rhodopsin deactivation

Consistent with earlier reports under similar conditions (Xu et al., 1997), individual flash families from WT and *Arr1*+/− rods were qualitatively similar (Fig. 2*A*). To more directly compare the response time courses, we calculated the average SPRs with variance-to-mean analysis from a large number ($n > 25$) of dim flash responses. An overlay of the population mean SPRs of WT and *Arr1*+/− rods revealed them to be nearly identical (Fig. 2*B*). Accordingly, the kinetic parameters of the dim flash response (time to peak, integration time, and time constant of recovery), which do not rely on variance-to-mean analysis, were all approximately the same for these rods (Table 1) ($p > 0.3$ for all metrics). Furthermore, the time-dependent variability of isolated SPRs in WT and *Arr1*+/− rods was similar in waveform, suggesting that SPR reproducibility is unaffected by underexpression of Arr1 (Fig. 2*C*). Thus, our more detailed characterization of *Arr1*+/− dim flash responses failed to reveal any effects of reduced Arr1 expression.

To test the idea that slowed Arr1 binding in *Arr1*+/− rods is obscured by still slower $G_t\alpha$/PDE deactivation, we recorded from Arr1-deficient rods that expressed the RGS9 complex at fourfold higher levels than normal (RGS9-ox; Krispel et al., 2006). In general, *Arr1*+/− $^{RGS9\text{-}ox}$ responses were larger and longer lasting than those of RGS9-ox rods, as revealed by representative flash families in Figure 3*A*. The population average SPR of *Arr1*+/− $^{RGS9\text{-}ox}$ rods continued to rise after the RGS9-ox SPR reached a peak (Table 1) ($p < 0.03$) (Fig. 3*B*,*C*). The rising phases of the average SPRs, which indicate the gain of the phototransduction cascade, followed a similar initial trajectory, as determined by the overlapping error bars (SEM) in Figure 3*C* and by measurement of the rate of change of the light-activated PDE activity (Pugh and Lamb, 1993). The longer time to peak therefore resulted in a larger SPR amplitude in the Arr1-underexpressing rods (Table 1) ($p < 0.001$) (Fig. 3*B*). Because the dark currents in these rods were indistinguishable ($p = 0.4$) (Table 1), an increased SPR amplitude suggests that a reduction of OS Arr1 content does lead to a reduced rate of Arr1-R* binding, and a longer average lifetime of R*.

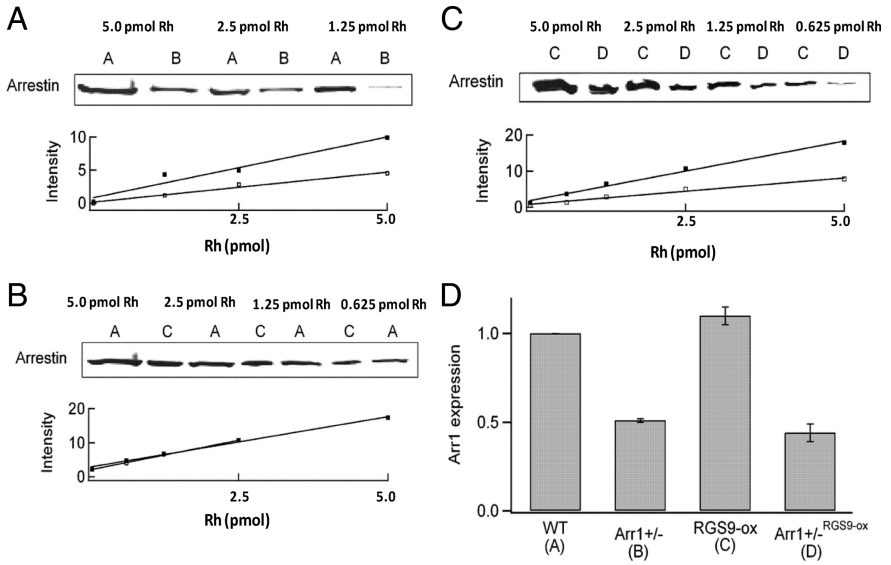


**Figure 1.** Arr1 expression is reduced by half in *Arr1*+/− and *Arr1*+/− $^{RGS9\text{-}ox}$ retinas. ***A***, Representative Western blot quantifying the expression of Arr1 in *Arr1*+/− retinal homogenate relative to wild-type. Total protein levels were estimated based on rhodopsin content, shown above each lane of the blot. Lanes labeled "A" were loaded with WT tissue (filled boxes in graph). "B" lanes were loaded with *Arr1*+/− tissue (empty boxes). The ratio of slopes (B/A) was 0.49. ***B***, Same as ***A***. "A" lanes were loaded with WT tissue (filled boxes); "C" were lanes loaded with RGS9-ox tissue (empty boxes). The ratio of slopes (C/A) was 1.2. ***C***, Same as ***A*** and ***B***. "C" lanes loaded with RGS9-ox tissue (filled boxes); "D" lanes loaded with *Arr1*+/− $^{RGS9\text{-}ox}$ tissue (empty boxes). The ratio of slopes (D/C) was 0.44. ***D***, Summary of Arr1 expression determined by quantitative Western blots. Relative expression levels were quantified as the ratio of the slopes of the lines that provided best fits for plots of Arr1 intensity versus rhodopsin content such as those in ***A–C***.

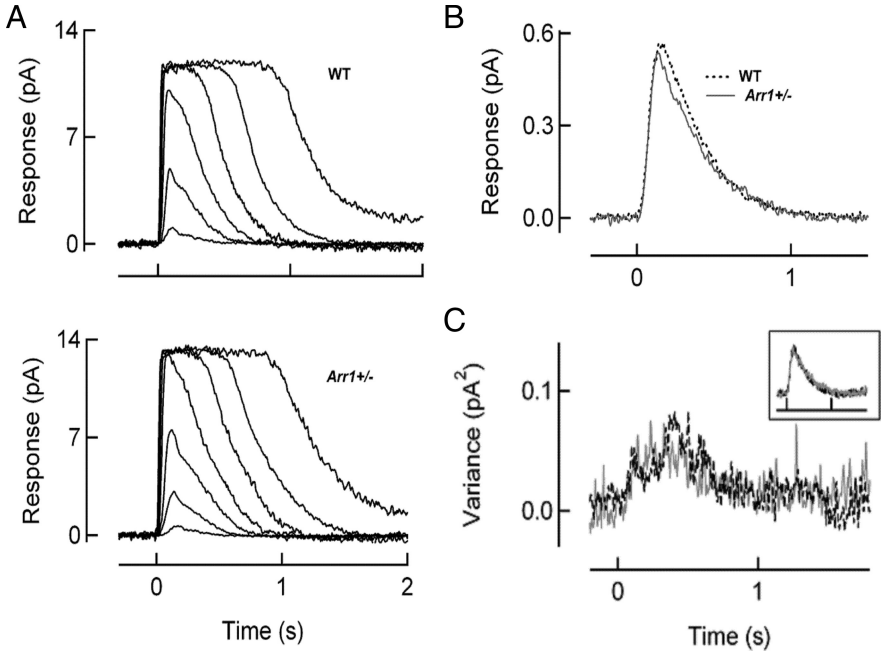


**Figure 2.** Underexpression of Arr1 does not affect time course or variability of single-photon responses in wild-type background. ***A***, Representative families of responses to flashes of light (500 nm, 10 ms, delivered at $t = 0$) that ranged from 6 to 6000 photons/$\mu m^2$ by factors of 4. Top, WT rod with 12.0 pA dark current. Bottom, *Arr1*+/− rod with 13.4 pA dark current. ***B***, Population mean single-photon responses of WT (dotted black line; $n = 19$) and *Arr1*+/− (solid gray line; $n = 17$) rods. ***C***, Mean time-dependent variances of isolated single-photon responses from subpopulations of WT and *Arr1*+/− rods ($n = 4$ for each genotype). Inset, Subpopulation mean single-photon responses for these rods used to generate time-dependent variances.

Further evidence for a longer R* lifetime in Arr1-deficient rods is provided by analysis of the recovery of RGS9-ox and

**Table 1. Characteristics of responses of rods with normal and reduced Arr1 expression**

| | Dark current (pA) | Elementary amplitude (pA) | Integration time (ms) | Time to peak (ms) | $\tau_{rec}$ (ms) | $\tau_D$ (ms) |
|---|---|---|---|---|---|---|
| Wild type | 13.3 ± 0.7 (19) | 0.61 ± 0.06 (19) | 360 ± 40 (17) | 141 ± 10 (19) | 220 ± 10 (18) | 204 ± 17 (8) |
| *Arr1+/−* | 12.2 ± 0.6 (19)[a] | 0.60 ± 0.08 (17)[a] | 350 ± 30 (16)[a] | 132 ± 7 (17)[a] | 240 ± 20 (16)[a] | 236 ± 17 (12)[a] |
| RGS9-ox | 13.4 ± 0.7 (20)[a] | 0.51 ± 0.03 (20)[c] | 150 ± 10 (17)[e] | 109 ± 5 (17)[d] | 76 ± 8 (17)[e] | 76 ± 3 (26)*,[e] |
| *Arr1+/−* $^{RGS9\text{-}ox}$ | 12.7 ± 0.5 (39)[a] | 0.75 ± 0.05 (35)[b,j] | 200 ± 10 (38)[e,g] | 128 ± 6 (39)[a,g] | 109 ± 8 (39)[e,h] | 79 ± 6 (19)[e,f] |

*Data reanalyzed from Krispel et al. (2006).

Statistical significance reported by Student's *t* tests was as follows: [a]$p > 0.2$ compared to WT; [b]$p = 0.08$ compared to WT; [c]$p = 0.14$ compared to WT; [d]$p = 0.01$ compared to WT; [e]$p < 0.001$ compared to WT; [f]$p > 0.6$ compared to RGS9-ox; [g]$p = 0.01$ compared to RGS9-ox; [h]$p = 0.003$ compared to RGS9-ox; [j]$p < 0.001$ compared to RGS9-ox.

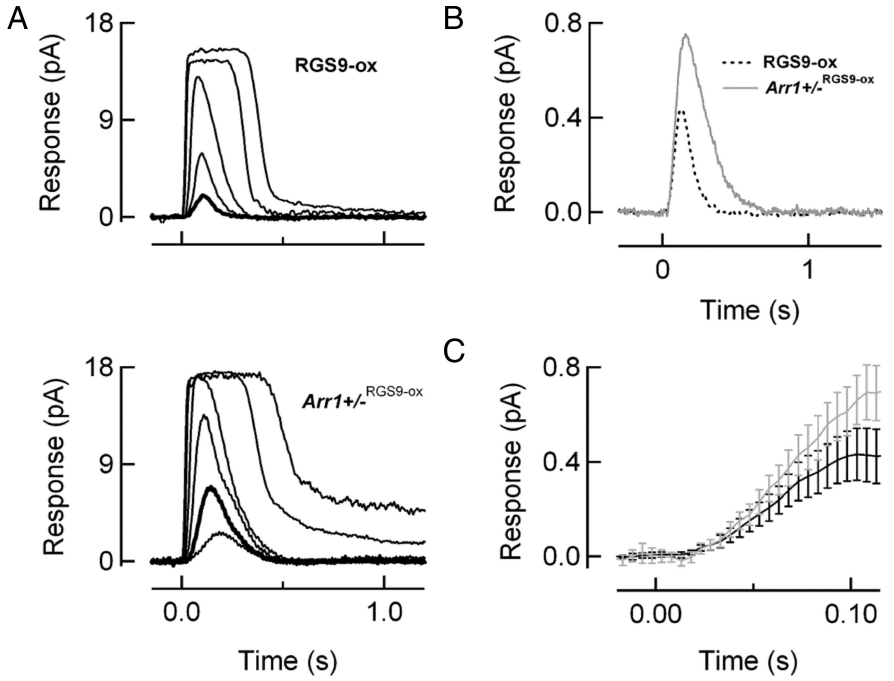


**Figure 3.** Underexpression of Arr1 results in slower recovery of photoresponses in RGS9-ox background. ***A***, Representative families of average responses to flashes that ranged in strength from 4 to 7000 photons/$\mu m^2$ by factors of 4. Top, RGS9-ox rod with 15.5 pA dark current. No responses to flash strengths of 4 or 600 photons/$\mu m^2$ were obtained. Bottom, *Arr1+/−* $^{RGS9\text{-}ox}$ rod with 17.5 pA dark current. Response to flash strength of 7000 photons/$\mu m^2$ not shown. In both panels, the bold trace indicates the average response to a flash of 16 photons/$\mu m^2$. ***B***, Population mean single-photon responses of RGS9-ox (dotted black line; $n = 14$) and *Arr1+/−* $^{RGS9\text{-}ox}$ (solid gray line; $n = 32$) rods. ***C***, Same as ***B*** but on an expanded time scale with range indicators depicting SEM (RGS9-ox in black; *Arr1+/−* $^{RGS9\text{-}ox}$ in gray).

*Arr1+/−* $^{RGS9\text{-}ox}$ dim flash responses. The final falling phase of the average dim flash response can be fit with a single-exponential function whose time constant $\tau_{rec}$ has a value of ~230 ms in WT and *Arr1+/−* rods (Table 1). This 230 ms value reflects the time constant for $G_t\alpha$/PDE deactivation and is reduced to 76 ms in rods that fourfold overexpress RGS9 (Krispel et al., 2006). Accelerated responses in RGS9-ox rods should reflect the time course of R* catalytic activity more closely than those of WT rods, and one would therefore expect that a sufficiently prolonged R* lifetime in the RGS9- ox background would increase $\tau_{rec}$. Indeed, *Arr1+/−* $^{RGS9\text{-}ox}$ responses recovered more slowly than RGS9-ox responses, with an average $\tau_{rec}$ of 109 ms (Fig. 3*B*, Table 1) ($p < 0.003$). Thus, we conclude that the reduced Arr1 levels in *Arr1+/−* $^{RGS9\text{-}ox}$ rods causes slowed rhodopsin deactivation.

The extent to which rhodopsin deactivation is slowed when Arr1 is underexpressed can be constrained by measurements of the dominant time constant of recovery for saturating flashes. This time constant, $\tau_D$, is given by the slope of the linear relationship between the time that bright flash responses remain in saturation ($T_{sat}$; >90% current suppression) and the natural logarithm of the number of photoisomerizations produced by the flashes (Pepperberg et al., 1992). In a previous study, we found that $\tau_D$, like $\tau_{rec}$, undergoes a shift from ~200 ms to ~80 ms in RGS9-ox rods (Krispel et al., 2006). In the present study, we found that $\tau_D$ is not larger for *Arr1+/−* $^{RGS9\text{-}ox}$ responses than for RGS9-ox responses (Fig. 4*A*, Table 1). Therefore, recovery of both *Arr1+/−* $^{RGS9\text{-}ox}$ and RGS9-ox saturating responses is dominated by the same ~80 ms time constant.

It is important to point out that we used no particular criteria for including or excluding cells in our analyses of either $\tau_D$ or $\tau_{rec}$; nevertheless, it was not always possible to obtain sufficient numbers of flash responses to determine both of these metrics in all cells. For the specific set of rods in which $\tau_{rec}$ and $\tau_D$ were both determined, the average values of $\tau_{rec}$ were 66 ± 6 ms ($n = 23$) and 102 ± 7 ms ($n = 19$) for RGS9-ox and *Arr1+/−* $^{RGS9\text{-}ox}$ rods, respectively ($p < 0.001$), and the average values of $\tau_D$ were 74 ± 3 ms and 79 ± 6 ms ($p = 0.4$). Why is there an increase in dim flash $\tau_{rec}$ for *Arr1+/−* $^{RGS9\text{-}ox}$ rods and yet no corresponding increase in $\tau_D$, when there is normally excellent correspondence between these two metrics (Chen et al., 2000), even when $G_t\alpha$/PDE deactivation has been dramatically speeded (Krispel et al., 2006; Chen et al., 2010; our results, Table 1)? The difference between $\tau_{rec}$ and $\tau_D$ in *Arr1+/−* $^{RGS9\text{-}ox}$ rods can be explained by careful examination of the time intervals over which the two metrics are determined. Because both R* and $G_t\alpha$/PDE deactivation proceed simultaneously, one must wait until "sufficiently long times" for the slower of these two steps to dominate response recovery, with the time required for dominance determined by the rates of R* and $G_t\alpha$/PDE deactivation (Nikonov et al., 1998). Our measurements of $\tau_{rec}$ begin as early as 180 ms after the flash in *Arr1+/−* $^{RGS9\text{-}ox}$ rods, while measurements of $\tau_D$ typically span the interval of 250–400 ms after the flash. While this latter time interval clearly fits the description of "sufficiently late times" because of the linearity of the semilog $T_{sat}$ relation (Fig. 4*A*), this criterion may not be met for the measurement of $\tau_{rec}$ when R* lifetime has been lengthened.

To investigate this idea further, we approximated the time course of the light-driven PDE activity $[E^*(t)]$ underlying the photoresponses as the convolution of two exponential decay functions describing R* and $G_t\alpha$/PDE decay ($\tau_R$ and $\tau_E$, respec-

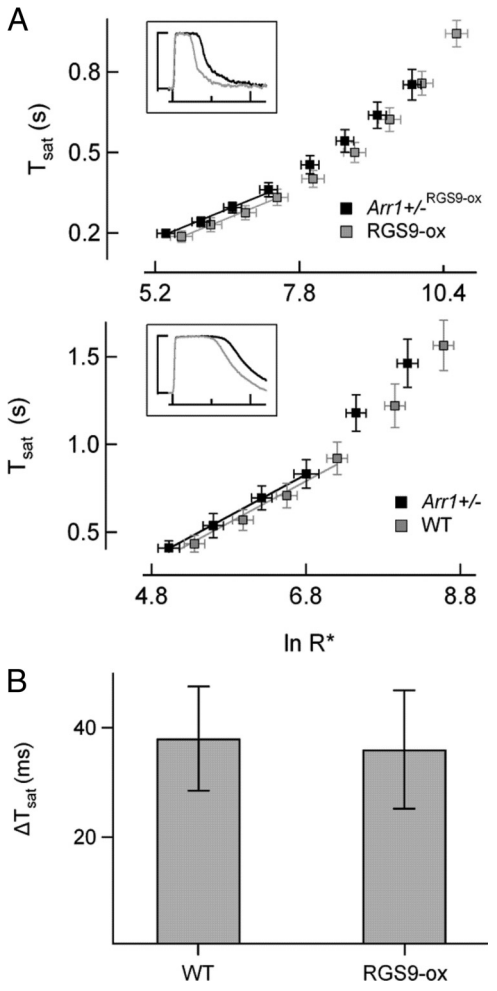


**Figure 4.** Saturating responses remain in saturation longer when Arr1 is underexpressed. ***A***, Top, The saturation times of responses resulting from 2500 or fewer photoisomerizations increased in proportion to the natural logarithm of R* for RGS9-ox [gray boxes; $n = 26$; slope = 83 ms; reanalyzed from Krispel et al. (2006)] and *Arr1*+/− $^{RGS9\text{-}ox}$ rods (black boxes; $n = 19$; slope = 86 ms). The slopes were not significantly different ($p > 0.5$). Inset, Examples of saturating flash responses that illustrate the difference in saturation times for individual RGS9-ox (750 R*; 16.3 pA dark current) and *Arr1*+/− $^{RGS9\text{-}ox}$ (700 R*; 17.1 pA dark current) rods. Bottom, Similar to top, with saturation times of responses to flashes that produced <1500 photoisomerizations for WT (gray boxes; $n = 8$; slope = 236 ms) and *Arr1*+/− rods (black boxes; $n = 12$; slope = 239). The slopes were not different ($p > 0.5$). Inset, Responses to saturating flashes of individual WT (640 R*; 14.5 pA dark current) and *Arr1*+/− (680 R*; 15.1 pA dark current) rods. ***B***, Underexpression of Arr1 resulted in nearly identical vertical offsets of the saturation times in WT (*Arr1*+/− vs WT, $\Delta T_{sat} = 38$ ms) and RGS9-ox backgrounds (*Arr1*+/− $^{RGS9\text{-}ox}$ vs RGS9-ox, $\Delta T_{sat} = 36$ ms), as depicted by the gray bars. Values conveyed by bar heights were calculated as the difference of the *y*-intercepts of lines fit to the data in ***A*** with slopes held fixed at 84 ms (RGS9-ox and *Arr1*+/− $^{RGS9\text{-}ox}$) or 238 ms (WT, *Arr1*+/−): $\Delta T_{sat} = y_0^{+/-} - y_0^{+/+}$. Range indicators represent 95% confidence intervals for the *y*-intercepts of the best-fit lines.

tively) and developed a mathematical relationship that defines the time $t_c$ at which dominance of the slower time constant is established (see Materials and Methods). A numerical value for $t_c$ can be fully determined by choosing values of $\tau_R$, $\tau_E$, and an error term ($\alpha = 0.1$) reflecting the fractional uncertainty in our measurements of $\tau_D$:

$$t_c - \frac{\tau_R \tau_E}{\tau_R - \tau_E} \ln\left[\frac{\alpha^2}{2\tau_R \tau_E}(2t_c^2 + 6t_c\tau_E + 5\tau_E^2)\right] = 0. \quad (4)$$

Letting $\tau_D = \tau_E = 80$ ms for rods that overexpress RGS9, a value of $\tau_R = 30$ ms yields $t_c = 83$ ms when Equation 4 is solved numerically for $t_c$. However, when the time constant for R* decay is doubled ($\tau_R = 60$ ms) to reflect a 50% decrease in Arr1 expression, Equation 4 yields $t_c = 271$ ms. This indicates that one would have to wait 271 ms after the flash in order for the final recovery phase of the photoresponse ($\tau_{rec}$) to reflect $\tau_E$ in the *Arr1*+/− $^{RGS9\text{-}ox}$ rods; by this time, the response has already recovered. In other words, $\tau_{rec}$ only reflects the slower of $\tau_R$ and $\tau_E$ if the two time constants are sufficiently different from each other. Importantly, when R* deactivation is normal ($\tau_R = 30$ ms), $t_c$ is sufficiently short (83 ms) so that $\tau_{rec}$ does match $\tau_D$, as observed in RGS9-ox rods. Thus, the dissimilarity of $\tau_{rec}$ and $\tau_D$ in *Arr1*+/− $^{RGS9\text{-}ox}$ rods ($p < 0.01$) further supports the conclusion that R* deactivation is slowed in rods that underexpress Arr1, and that this prolonged R* lifetime is still shorter than the 80 ms lifetime of $G_t\alpha$/PDE.

Although the slopes ($\tau_D$) of the $T_{sat}$ relations were the same, the absolute times that responses remained in saturation were consistently longer in Arr1+/− $^{RGS9\text{-}ox}$ than in RGS9-ox rods, resulting in an ~40 ms vertical offset of the $T_{sat}$ values (Fig. 4*A*). Remarkably, examination of the $T_{sat}$ relations of *Arr1*+/− and wild-type responses (Fig. 4*A*, bottom) showed the same ~40 ms vertical offset (Fig. 4*B*). This offset could not be explained by subtle differences in the rods' collecting areas or flash sensitivities, which were directly measured in each cell (see Materials and Methods). The fact that Arr1 underexpression resulted in the same 40 ms offset in both WT and RGS9-overexpressing backgrounds suggests that the reduced Arr1 expression slowed rhodopsin deactivation to the same extent in the two genetic backgrounds.

### Deduction of the rates of phosphorylation and Arr1 binding for rhodopsin deactivation

While $\tau_D$ is a convenient measure of the slowest, "dominant" time constant, the absolute time that a bright flash response remains in saturation can provide information about R* decay (i.e., the "nondominant time constant") (Nikonov et al., 2000). All other parameters being equal, the increase in saturation times that we observed in Arr1-underexpressing rods limits the magnitude of the increase in the lifetime of R*. For the two-time constant model discussed above (Eq. 3 in Materials and Methods), the 40 ms change in the absolute time in saturation is consistent with only a small increase in R* lifetime (8–17% increase in R* lifetime from a WT value between 80 and 20 ms). However, since R* deactivation is a multistep process in which Arr1 binding occurs only after phosphorylation has partially reduced R* activity (Gurevich, 1998; Gibson et al., 2000; Vishnivetskiy et al., 2007), such a simple first-order scheme that is entirely dependent on Arr1 binding seems inappropriate. Instead, we adopted a double-exponential scheme for R* deactivation, with the two components representing the time courses of phosphorylation and Arr1 binding, and assumed that underexpression of Arr1 would affect only Arr1 binding.

Thus, the centerpiece of our revised model is a $G_t\alpha$/PDE pulse [$E^*(t)$] defined by three time constants corresponding to the time courses of R* phosphorylation ($\tau_k$), R* quench by Arr1 ($\tau_a$), and $G_t\alpha$/PDE deactivation ($\tau_E$):

$$R^*(t) = A_a e^{-t/\tau_a} + A_k e^{-t/\tau_k}$$

$$E^*(t) = R^*(t) * (\nu_{RE}\, e^{-t/\tau_E}). \quad (5)$$

The star (*) in Equation 5 indicates a convolution operation. Because $\tau_E$ is experimentally determined as the dominant time constant of recovery, the only free parameters in this equation are

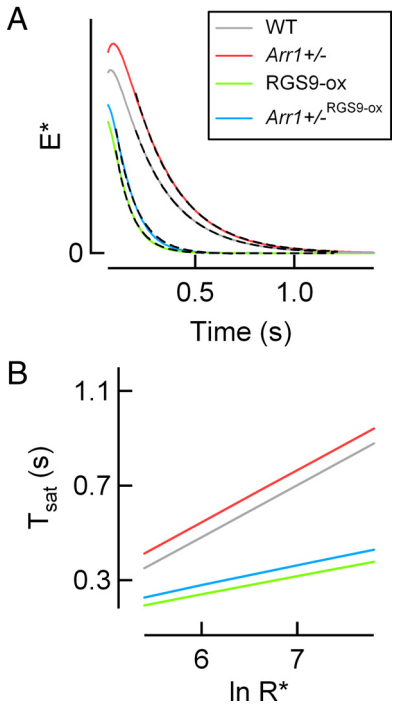


**Figure 5.** Two-stage model of rhodopsin deactivation captures time course of photoresponse recovery associated with underexpression of Arr1. ***A***, The double-exponential function for rhodopsin decay (Eq. 5) was used to simulate the decline of $G_t\alpha$/PDE in WT, *Arr1*+/−, RGS9-ox, and *Arr1*+/− $^{RGS9\text{-}ox}$ rods. The time constant for $G_t\alpha$/PDE decay was set according to measurements of $\tau_D$ (75 ms for RGS9-ox and *Arr1*+/− $^{RGS9\text{-}ox}$ traces; 220 ms for WT and *Arr1*+/− traces). The time constants $\tau_k$ and $\tau_a$ were set to the best-fit values described in Results ($\tau_k = 36$ ms for all traces; $\tau_a = 36$ ms for WT and RGS9-ox traces; $\tau_a = 67$ ms for *Arr1*+/− $^{RGS9\text{-}ox}$ and *Arr1*+/− traces). The ratio of exponential amplitudes $A_a/A_k$ was 0.4, as determined by saturation time data. Black traces are single-exponential functions fit to the theory, and had time constants similar to the experimentally measured values of $\tau_{rec}$ across the same time interval for the corresponding genotype (WT, 221 ms; *Arr1*+/−, 227 ms; RGS9-ox, 85 ms; *Arr1*+/− $^{RGS9\text{-}ox}$, 104 ms) (compare with Table 1). ***B***, Time in saturation ($T_{sat}$) as a function of natural log R* for each simulated genetic line, obtained by scaling $G_t\alpha$/PDE pulses of Figure 5*A* by the desired number of R*, and considering each to be in saturation until they fell to an arbitrary but constant criterion level of E* activity. The slopes of the resulting lines were quantitatively similar to experimental measurements shown in Figure 4. Specifically, the slopes of the WT and *Arr1*+/− traces were ~220 ms, and those of the RGS9-ox and *Arr1*+/− $^{RGS9\text{-}ox}$ traces were ~80 ms. Furthermore, the *Arr1*+/− $^{RGS9\text{-}ox}$ trace had a 40 ms vertical displacement relative to the RGS9-ox trace, and the *Arr1*+/− trace was offset from the WT trace by 50 ms.

$\tau_k$ and $\tau_a$. The amplitude ratio of the contributing terms ($A_a/A_k$) is determined by the values of the time constants $\tau_k$ and $\tau_a$ and the observed 40 ms increase in saturation times (Fig. 4; see Materials and Methods). The rate constant for the activation of $G_t\alpha$/PDE by R*, $\nu_{RE}$, affects the amplitude of $E^*(t)$ but has no consequence for our results relating to the time course of recovery. The values of $\tau_k$ and $\tau_a$ were each allowed to vary between 0 and 80 ms, and for each pair, a numerical score was calculated based upon the similarity of the final falling phases of the modeled $E^*(t)$ pulses and the observed $\tau_{rec}$ data (Fig. 5*A*) over the same time window. Our *Arr1*+/− data provided strong constraints for this model, with best-fitting values $\tau_k = 36$ ms and $\tau_a^{+/-} = 67$ ms (for details on fitting process, see supplemental material, available at www.jneurosci.org). Thus, when Arr1 levels are one-half of normal, the time constant for R* phosphorylation is 36 ms, and that of Arr1 binding is 67 ms. If Arr1 binding becomes approximately twofold faster when Arr1 expression is doubled to the WT level, then the representation of R* decay in our model reduces to a single-exponential function with $\tau_a^{wt} = \tau_k = 36$ ms for responses of rods with normal Arr1 expression. Indeed, this parameterization produced $E^*(t)$ time courses that were statistically equivalent to the experimental measurements of $\tau_D$ and $\tau_{rec}$ from WT and RGS9-ox rods (Fig. 5). To further test whether the double-exponential scheme for R* deactivation was sufficient to explain the experimental observations, the fitting procedure was performed a second time as described above, except that the assumption $\tau_a^{wt} = \tau_k$ was replaced with the assumption $\tau_a^{+/-} = 2\tau_a^{wt}$, so that the free parameters for this fitting procedure were $\tau_k$ and $\tau_a^{wt}$. Importantly, the best-fit values determined with this alternate assumption were extremely close to the values reported for the first fitting procedure ($\tau_k = 36$ ms, $\tau_a^{+/-} = 2\tau_a^{wt} = 68$ ms). The score for the pair of best-fit values was slightly worse than that produced by the parameter values determined under the original assumptions.

In summary, this simple model based on the idea that R* decay can be represented as a double-exponential function in which phosphorylation proceeds independently of the rate of Arr1 binding is able to capture seemingly disparate results of response recovery in both dim and saturating flash regimes of our four mouse lines. A single set of three parameters ($\tau_k$, $\tau_a^{wt}$, $\tau_a^{+/-}$) can quantitatively account for all six major features of our recovery kinetic data, including (1) the difference in $\tau_{rec}$ and (2) the similarity in $\tau_D$ for RGS9-ox and *Arr1*+/− $^{RGS9\text{-}ox}$ responses, the similarity in both (3, 4) $\tau_{rec}$ and $\tau_D$ for WT and *Arr1*+/− responses, and (5, 6) the increase in $T_{sat}$ for both *Arr1*+/− $^{RGS9\text{-}ox}$ and *Arr1*+/− saturating responses relative to RGS9-ox and WT saturating responses, respectively.

## Discussion

### Estimation of R* lifetime: the dependence on Arr1 expression

Overexpression of the RGS9 complex dramatically accelerates recovery of both dim and saturating flash responses, indicating that $G_t\alpha$/PDE deactivation normally rate-limits recovery and setting an upper bound on the lifetime of R* (Krispel et al., 2006; Chen et al., 2010). The highest overexpression of RGS9 achieved to date indicates that in dark-adapted rods, R* deactivation proceeds with a time constant of ≤54 ms (Chen et al., 2010), and theoretical work suggests that it is probably <50 ms (Burns and Pugh, 2009). The results in this study further support the idea of a short R* lifetime: our data and analysis show that in normal rods, R* deactivation proceeds with a time constant equal to 36 ms.

Our analysis suggests that in wild-type rods the outer segment level of Arr1 is such that phosphorylation and Arr1 binding proceed at approximately the same rates, allowing R* deactivation to be well approximated by a single exponential. The similarity in these rates should help to make the pulse of R* activity more similar from trial to trial, which is thought to be important for the reproducibility of the single-photon response (Rieke and Baylor, 1998). A biochemically realistic mathematical model for reproducibility that incorporates faster R* deactivation will be necessary to understand the significance, or coincidence, of the similarity in these rates of phosphorylation and arrestin binding in normal rods. To date, the shortest R* lifetime that has been used in modeling reproducibility is 118 ms (Bisegna et al., 2008).

Our results directly contradict a recent study (Doan et al., 2009), which reported that R* deactivation rate-limits recovery, and that R* deactivation is slightly faster when Arr1 is underexpressed. Doan et al. (2009) proposed that their findings may have been unique to their recording conditions, which used Ames' medium rather than Locke's. However, we found that RGS9

overexpression dramatically accelerates response recovery more than twofold in Ames' medium (supplemental Fig. S2, available at www.jneurosci.org as supplemental material), similar to what has been reported in Locke's solution (Krispel et al., 2006; this present study) and in Eagle's medium (Chen et al., 2010). Thus, $G_t\alpha$/PDE deactivation remains rate limiting even in Ames' medium. By extension, the conclusion of Doan et al. (2009) that R* deactivation is 22% faster in *Arr1+/−* rods is likewise refuted by the dramatic effect of RGS9-overexpression in Ames, and their competition model for R* deactivation, which is based on a long R* lifetime, cannot be correct. [Further discussion of Doan et al. (2009) is provided in the supplemental material, available at www.jneurosci.org.] In contrast, our results support a traditional biochemical scheme in which the rate of phosphorylation is independent of Arr1 concentration, and lowering Arr1 concentration slows R* deactivation slightly by reducing the rate of Arr1 binding.

The slowed rate of Arr1 binding in *Arr1+/−* rods can be used to estimate the concentration of Arr1 available to bind R* in dark-adapted mouse outer segments. Biochemical studies have indicated that the association rate constant for Arr1 and phosphorylated R* is $\sim 1\ \mu M^{-1} \cdot s^{-1}$ (Schleicher et al., 1989; Pulvermüller et al., 1997). In rods with reduced Arr1 expression, our calculated Arr1 binding rate of $15\ s^{-1}$ (1/67 ms) corresponds to an effective OS Arr1 concentration of 15 $\mu$M in *Arr1+/−* rods. For wild-type rods with a binding rate of at least $28\ s^{-1}$ (1/36 ms), the corresponding calculation yields an effective Arr1 concentration of at least 28 $\mu$M, which is close to previous estimates for endogenous OS Arr1 monomer in bovine rods (Gurevich et al., 2007).

Our conclusion that the rate of Arr1 binding changes in nearly direct proportion to a change in total OS Arr1 content is at odds with the emerging notion that the amount of free Arr1 available to bind R* is buffered through oligomerization (Gurevich et al., 2007; Hanson et al., 2007a; Hanson et al., 2007b). Dissociation constants for bovine Arr1 determined at room temperature for the formation of Arr1 dimers and tetramers predicts that the 1.9-fold reduction in Arr1 monomer concentration calculated above would be accompanied by a fourfold reduction in total Arr1 expression, rather than the 1.8-fold that we observe experimentally (supplemental Fig. S1, available at www.jneurosci.org as supplemental material). Our results suggest that the $K_d$ for dimerization of mouse Arr1 at physiological temperatures must be significantly greater than that determined for bovine Arr1 (Hanson et al., 2007a), so that the amount of available Arr1 monomer, and thus the rate of Arr1 binding, does indeed vary as the total Arr1 content of the outer segment changes.

### Implications for light-dependent movement of Arr1

The total Arr1 content in the outer segment changes dramatically with light exposure (for review, see Calvert et al., 2006). In mouse rods, the OS Arr1 concentration can vary as much as ~10-fold between dark-adapted conditions and light exposures that activate ~3% of the total rhodopsin over a span of 10 min (Strissel et al., 2006). Our results on dark-adapted rods can also be used to estimate the functional consequences that Arr1 translocation of this magnitude would have on R* lifetime. Under our simple model, the rate of Arr1 binding to phosphorylated R* would increase nearly in proportion to the increase in OS Arr1 content, predicting that $\tau_a$ would decrease from 36 ms to ~4 ms. If the rate of phosphorylation is unaffected, the integrated PDE activity from a given flash response would decrease by only 24%. Thus, even large (10-fold) changes in Arr1 levels are predicted to produce only modest changes in flash responses. (Here we are focused only on R* deactivation, rather than any effect of Arr1 levels on amplification through competition with $G_t\alpha$ for R*.) Our calculation suggests that the time course with which R* activity decays is primarily determined by phosphorylation, because the phosphorylation rate determines Arr1 binding independently of Arr1 content.

### Control of the single-photon response amplitude by Arr1 expression in RGS9-overexpressing rods

In addition to the noted effects on recovery kinetics, underexpression of Arr1 increased the SPR amplitude in the RGS9-ox background, but not the wild-type background (Table 1). A similar observation was also made in a recent study that showed that sensitivity was unchanged when R* lifetime was lengthened by underexpressing GRK1 in the wild-type background, but that it was substantially increased by GRK1 underexpression in the RGS9 overexpression background (Chen et al., 2010). We propose that this differential effect of R* lifetime in WT and RGS9-ox backgrounds stems from differences in the calcium-dependent regulation of cGMP synthesis, which strongly affects SPR amplitude (Burns et al., 2002). For example, if the dark PDE activity is reduced in rods that overexpress RGS9, then the dark calcium levels would be slightly elevated and the dark rate of cGMP synthesis would also be reduced. As a consequence, there would be less activation of guanylate cyclase in response to the change in calcium that accompanies the flash response in RGS9-ox rods, unmasking the lengthened R* lifetime associated with Arr1 underexpression. Conversely, in the WT background higher rates of cGMP synthesis during the light response dampen small increases or decreases in R* lifetime more strongly. This mechanism may explain why sensitivity is preserved in rods that overexpress GRK1 (Krispel et al., 2006; Whitcomb et al., 2009) or lack the GRK1 inhibitory protein, recoverin (Makino et al., 2004).

### Estimation of the rate of rhodopsin phosphorylation in wild-type rods

Our double-exponential model suggests that in wild-type rods, phosphorylation by GRK1 initially decreases R* activity with an overall rate of $\sim 28\ s^{-1}$ (1/36 ms). Importantly, the rate provided by this model does not address the number of phosphorylations that precede Arr1 binding, since the durations of each progressive GRK1 binding event and phosphate transfer leading to Arr1 quench are rolled into the aggregate time constant. While several electrophysiology studies have suggested that 3–6 phosphorylation sites are necessary for normal deactivation of R* (Mendez et al., 2000; Doan et al., 2006), biochemical studies show that two of these sites need to be phosphorylated to increase the affinity of Arr1 appreciably and that a minimum of three phosphorylations are required for high-affinity binding (Vishnivetskiy et al., 2007). Perhaps the extra phosphorylation sites at the flexible, relatively unstructured C terminus of rhodopsin (Palczewski et al., 2000; Park et al., 2008) increase the rate of phosphorylation by increasing the local substrate for GRK1. Faster phosphorylation associated with an excess of possible phosphorylation sites would lead to more rapid Arr1 binding and consequently faster overall R* deactivation. Testing this idea would further tease apart the relative rates of phosphorylation and arrestin binding, which is essential for understanding the balance between signal amplification and rapid, reliable recovery in rods.

## References


Arshavsky VY, Lamb TD, Pugh EN Jr (2002) G proteins and phototransduction. Annu Rev Physiol 64:153–187.

Baylor DA, Lamb TD, Yau KW (1979) Responses of retinal rods to single photons. J Physiol 288:613–634.

Bisegna P, Caruso G, Andreucci D, Shen L, Gurevich VV, Hamm HE, DiBenedetto E (2008) Diffusion of the second messengers in the cytoplasm acts as a variability suppressor of the single photon response in vertebrate phototransduction. Biophys J 94:3363–3383.

Burns ME, Mendez A, Chen J, Baylor DA (2002) Dynamics of cyclic GMP synthesis in retinal rods. Neuron 36:81–91.

Burns ME, Pugh EN Jr (2009) RGS9 concentration matters in rod phototransduction. Biophys J 97:1538–1547.

Calvert PD, Strissel KJ, Schiesser WE, Pugh EN Jr, Arshavsky VY (2006) Light-driven translocation of signaling proteins in vertebrate photoreceptors. Trends Cell Biol 16:560–568.

Chan S, Rubin WW, Mendez A, Liu X, Song X, Hanson SM, Craft CM, Gurevich VV, Burns ME, Chen J (2007) Functional comparisons of visual arrestins in rod photoreceptors of transgenic mice. Invest Ophthalmol Vis Sci 48:1968–1975.

Chen CK, Burns ME, Spencer M, Niemi GA, Chen J, Hurley JB, Baylor DA, Simon MI (1999) Abnormal photoresponses and light-induced apoptosis in rods lacking rhodopsin kinase. Proc Natl Acad Sci U S A 96:3718–3722.

Chen CK, Burns ME, He W, Wensel TG, Baylor DA, Simon MI (2000) Slowed recovery of rod photoresponse in mice lacking the GTPase accelerating protein RGS9-1. Nature 403:557–560.

Chen C-K, Woodruff ML, Chen FS, Chen D, Fain GL (2010) Background light produces a recoverin-dependent modulation of activated-rhodopsin lifetime in mouse rods. J Neurosci 30:1213–1220.

Doan T, Mendez A, Detwiler PB, Chen J, Rieke F (2006) Multiple phosphorylation sites confer reproducibility of the rod's single-photon responses. Science 313:530–533.

Doan T, Azevedo AW, Hurley JB, Rieke F (2009) Arrestin competition influences the kinetics and variability of the single-photon responses of mammalian rod photoreceptors. J Neurosci 29:11867–11879.

Gibson SK, Parkes JH, Liebman PA (2000) Phosphorylation modulates the affinity of light-activated rhodopsin for G protein and arrestin. Biochemistry 39:5738–5749.

Gurevich VV (1998) The selectivity of visual arrestin for light-activated phosphorhodopsin is controlled by multiple nonredundant mechanisms. J Biol Chem 273:15501–15506.

Gurevich VV, Hanson SM, Gurevich EV, Vishnivetskiy SA (2007) How rod arrestin achieved perfection: regulation of its availability and binding selectivity. In: Signal transduction in the retina (Fliesler SJ, Kisselev O, eds), pp 55–88. Boca Raton, FL: CRC.

Hanson SM, Gurevich EV, Vishnivetskiy SA, Ahmed MR, Song X, Gurevich VV (2007a) Each rhodopsin molecule binds its own arrestin. Proc Natl Acad Sci U S A 104:3125–3128.

Hanson SM, Van Eps N, Francis DJ, Altenbach C, Vishnivetskiy SA, Arshavsky VY, Klug CS, Hubbell WL, Gurevich VV (2007b) Structure and function of the visual arrestin oligomer. EMBO J 26:1726–1736.

Heck M, Hofmann KP (2001) Maximal rate and nucleotide dependence of rhodopsin-catalyzed transducin activation: initial rate analysis based on a double displacement mechanism. J Biol Chem 276:10000–10009.

Keresztes G, Martemyanov KA, Krispel CM, Mutai H, Yoo PJ, Maison SF, Burns ME, Arshavsky VY, Heller S (2004) Absence of the RGS9.Gbeta5 GTPase-activating complex in photoreceptors of the R9AP knockout mouse. J Biol Chem 279:1581–1584.

Krispel CM, Chen D, Melling N, Chen YJ, Martemyanov KA, Quillinan N, Arshavsky VY, Wensel TG, Chen CK, Burns ME (2006) RGS expression rate-limits recovery of rod photoresponses. Neuron 51:409–416.

Krupnick JG, Gurevich VV, Benovic JL (1997) Mechanism of quenching of phototransduction. Binding competition between arrestin and transducin for phosphorhodopsin. J Biol Chem 272:18125–18131.

Makino CL, Dodd RL, Chen J, Burns ME, Roca A, Simon MI, Baylor DA (2004) Recoverin regulates light-dependent phosphodiesterase activity in retinal rods. J Gen Physiol 123:729–741.

Mendez A, Burns ME, Roca A, Lem J, Wu LW, Simon MI, Baylor DA, Chen J (2000) Rapid and reproducible deactivation of rhodopsin requires multiple phosphorylation sites. Neuron 28:153–164.

Nikonov S, Engheta N, Pugh EN Jr (1998) Kinetics of recovery of the dark-adapted salamander rod photoresponse. J Gen Physiol 111:7–37.

Nikonov S, Lamb TD, Pugh EN Jr (2000) The role of steady phosphodiesterase activity in the kinetics and sensitivity of the light-adapted salamander rod photoresponse. J Gen Physiol 116:795–824.

Palczewski K, Rispoli G, Detwiler PB (1992) The influence of arrestin (48K protein) and rhodopsin kinase on visual transduction. Neuron 8:117–126.

Palczewski K, Kumasaka T, Hori T, Behnke CA, Motoshima H, Fox BA, Le Trong I, Teller DC, Okada T, Stenkamp RE, Yamamoto M, Miyano M (2000) Crystal structure of rhodopsin: a G protein-coupled receptor. Science 289:739–745.

Park JH, Scheerer P, Hofmann KP, Choe HW, Ernst OP (2008) Crystal structure of the ligand-free G-protein-coupled receptor opsin. Nature 454:183–187.

Pepperberg DR, Cornwall MC, Kahlert M, Hofmann KP, Jin J, Jones GJ, Ripps H (1992) Light-dependent delay in the falling phase of the retinal rod photoresponse. Vis Neurosci 8:9–18.

Pugh EN Jr, Lamb TD (1993) Amplification and kinetics of the activation steps in phototransduction. Biochim Biophys Acta 1141:111–149.

Pulvermüller A, Maretzki D, Rudnicka-Nawrot M, Smith WC, Palczewski K, Hofmann KP (1997) Functional differences in the interaction of arrestin and its splice variant, p44, with rhodopsin. Biochemistry 36:9253–9260.

Rieke F, Baylor DA (1998) Origin of reproducibility in the responses of retinal rods to single photons. Biophys J 75:1836–1857.

Schleicher A, Kühn H, Hofmann KP (1989) Kinetics, binding constant, and activation energy of the 48-kDa protein-rhodopsin complex by extrametarhodopsin II. Biochemistry 28:1770–1775.

Strissel KJ, Sokolov M, Trieu LH, Arshavsky VY (2006) Arrestin translocation is induced at a critical threshold of visual signaling and is superstoichiometric to bleached rhodopsin. J Neurosci 26:1146–1153.

Vishnivetskiy SA, Raman D, Wei J, Kennedy MJ, Hurley JB, Gurevich VV (2007) Regulation of arrestin binding by rhodopsin phosphorylation level. J Biol Chem 282:32075–32083.

Whitcomb TL, Sakurai K, Brown BM, Young JE, Sheflin L, Dlugos C, Craft CM, Kefalov VJ, Khani SC (2009) Effect of G protein-coupled receptor kinase 1 (Grk1) overexpression on rod photoreceptor cell viability. Invest Ophthalmol Vis Sci. Advance online publication. Retrieved Feb. 19, 2010. doi:10.1167/iovs.09-4499.

Xu J, Dodd RL, Makino CL, Simon MI, Baylor DA, Chen J (1997) Prolonged photoresponses in transgenic mouse rods lacking arrestin. Nature 389:505–509.